J. Phys.: Condens. Matter **9** (1997) 6563–6577. Printed in the UK PII: S0953-8984(97)81360-4

Crystal structure and paramagnetic behaviour of ε-WO_{3-x}

Ekhard K H Salje†‡♯, Stephan Rehmann§♯, Frank Pobell§[+], Darryl Morris†[*]♯, Kevin S Knight‖♯, Thomas Herrmannsdörfer§¶♯ and Martin T Dove†♯

† Department of Earth Sciences, University of Cambridge, Downing Street, Cambridge CB2 3EQ, UK

‡ Interdisciplinary Research Centre in Superconductivity, University of Cambridge, Madingley Road, Cambridge, UK

§ Lehrstruhl Experimentalphysik V, Universität Bayreuth, D-95440 Bayreuth, Germany

‖ ISIS Facility, Rutherford Appleton Laboratory, Chilton, Didcot, Oxfordshire OX11 0QX, UK

¶ Hahn–Meitner Institut Berlin, Glienicker Strasse 100, D-14109 Berlin, Germany

Received 28 January 1997, in final form 16 May 1997

Abstract. The crystal structure of the lowest-temperature ε-phase of WO_3 has been determined as a function of temperature by neutron powder diffraction. The diffraction measurements show that there are no additional phases at low temperatures. Magnetic measurements suggest that no superconductivity exists at temperatures as low as 9×10^{-5} K, but instead, an increase of the magnetic susceptibility according to a paramagnetic Curie law was found. This observation indicates that unpaired carriers persist in the sample after cooling to very low temperatures.

1. Introduction

The physical properties of tungsten trioxide, WO_3, and its slightly oxygen-deficient analogues, WO_{3-x}, have attracted renewed attention because their electronic properties may shed some light on one possible pairing mechanism in high-temperature superconductors, namely Bose condensation of pre-formed bipolaron charge carriers [1–12]. Experimental suggestions of possible Bose condensation stem from the departure of the nuclear spin-relaxation rate from the Korringa law [3], the heat capacity anomaly [4, 5], and the softening of phonons above the pseudo-gap in the superconducting phase [7, 8, 13–15].

Any experimental investigation of possible (bi-) polaron states in high-temperature superconductors is notoriously difficult because the high carrier density and the simultaneous existence of fermionic carriers [16–20] make it hard to observe signals which are clearly correlated with isolated polarons. Low carrier concentrations in purely polaronic systems without obvious spatial clustering of the carriers represents an ideal and, indeed, very rare physical situation. It is generally expected that WO_{3-x} is a material that will present such an exceptional situation [20–26].

WO_{3-x} possesses several crystallographic phases—here we are mainly concerned with the low-temperature ε-phase. The effective mass of the bosonic bipolarons in ε-WO_{3-x}

[+] Present address: Forschungszentrum Rossendorf, D-01314 Dresden, Germany.

[*] Present address: Department of Physics, University of York, Heslington, York YO1 5DD, UK.

♯ E-mail addresses: E K H Salje: es10001@esc.cam.ac.uk; S Rehmann: stephan@btp9x4.phy.uni-bayreuth.de; D Morris: dwsm100@york.ac.uk; K S Knight: ksk@isise.rl.ac.uk; T Herrmannsdörfer: thomas.herrmannsdorfer@uni-bayreuth.de; and M T Dove: martin@minp.esc.cam.ac.uk.

0953-8984/97/316563+15$19.50 © 1997 IOP Publishing Ltd

was previously estimated as $m^{**}_{\text{bipolaron}} = 1.9m_e$ [27]. Using the equation for non-interacting particles,

$$k_B T_c = 3.3\hbar^2 n^{2/3}/m^{**}$$

we obtain a value for the condensation temperature $T_c \sim 15$ K with $n \approx 10^{18}$ cm^{-3}. If, on the other hand, the bipolaron mass increases with decreasing temperature to that of other perovskite superconductors (e.g. $m^{**}_{\text{bipolaron}} = 240m_e$ in cubic bismuth compounds), we expect $T_c \sim 0.1$ K. We report in this paper that no superconductivity was observed at temperatures as low as 9×10^{-5} K, but instead, an increase of the magnetic susceptibility according to a paramagnetic Curie law was found. This observation indicates that unpaired carriers persist in the sample after cooling to very low temperatures.

The question arises of whether the unpaired states are correlated with another structural modification of WO_{3-x} at temperatures below the known δ–ε phase transitions, as claimed by Lefkowitz *et al* [28]. Indeed, these authors suggested that additional phase transitions exist at 40, 65, 130, 220 and 260 K. We have determined the crystal structure of WO_{3-x} in the temperature interval between 20 K and room temperature and found no additional structural phases besides ε-WO_{3-x} at low temperatures. This observation shows that the absence of pairing amongst the carriers is not related to any changes of the crystal structure of WO_{3-x}.

2. Experimental details

2.1. Sample preparation

A polycrystalline sample was prepared by annealing commercial WO_3 powder in a Pt crucible at 800 °C for two days and subsequent rapid heating to 1480 °C. The sample was left at that temperature for two hours and then cooled over two days to room temperature. The product consisted of a coarse-grained ceramic of WO_3, similar to those described previously [21, 22]. The colour of the sample was greenish yellow. Earlier work found carrier concentrations in samples prepared in the same way of (8–13) $\times 10^{18}$ cm^{-3} [21], but this concentration depends on the exact nature of the carriers. Our measurements reported below suggest that when pairing is taken into account, the carrier concentration for the samples used in this work is rather lower (0.33×10^{18} cm^{-3}), which leads to a value of x for the oxygen content in the notional formula WO_{3-x} of order 2×10^5. The samples used in both of the experimental studies reported in this paper were taken from the same batch of material.

2.2. Neutron diffraction

Approximately 5 cm^3 of the sample were carefully ground by hand; special care is needed because finely ground samples can sometimes fail to transform in the same way as bulk samples. The powdered sample was loaded into a rectangular can with vanadium windows, which was then mounted in a He-flow cryostat.

The neutron powder diffraction data were obtained using the high-resolution time-of-flight powder diffractometer at the ISIS pulsed spallation neutron source. Data were collected for times of flight between 30 and 130 ms, corresponding to d-spacings between about 0.6 and 2.6 Å. Data were collected in steps of 10 K from 20–240 K, with some long counting times and some shorter counting times. Additional data were collected on cooling again. Although the accuracy of the data for the shorter counting times is necessarily lower,

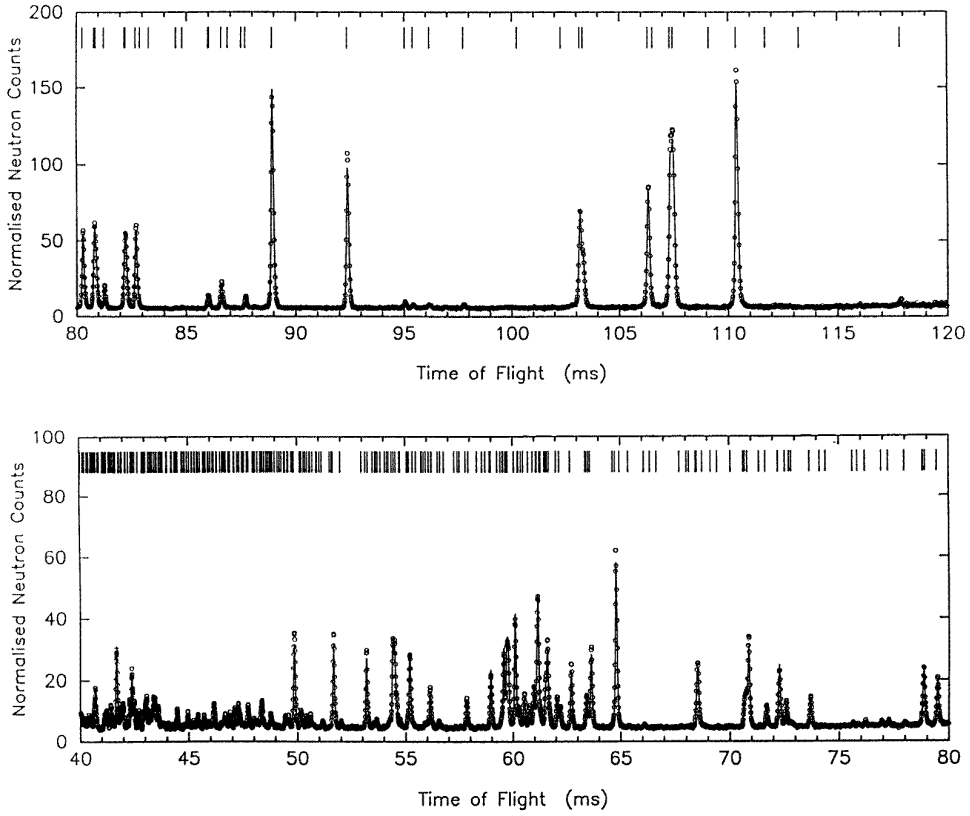

Figure 1. Observed (●) and calculated (——) diffraction patterns of WO_3 at 5 K. Details of the experimental measurement are given in the text.

the data were still of sufficient quality to allow good Rietveld analysis. For most of the data the diffraction patterns could be indexed as a single monoclinic phase using the cell parameters deduced by Salje [29] for ε-WO_3, space group Pc. Above 220 K the diffraction patterns contained both the low-temperature monoclinic ε-phase and the higher-temperature triclinic δ-phase [30, 31]. On cooling, the sample transformed back to the single-phase monoclinic form. All of the data were collected within 24 hours.

The data were normalized against the spectrum of the incident beam as measured by a monitor detector located in front of the sample. The instrument contains 20 rings of detectors in the back-scattering positions, and the spectra from all of the detectors were corrected for electronic noise and merged using in-house software. Because tungsten has a small but significant absorption cross section (18.4 b, to be compared with the coherent scattering cross sections of 5.7 b for tungsten and 4.2 b for oxygen), the data were corrected for beam attenuation using in-house software.

2.3. Magnetic susceptibility measurements

The magnetic susceptibility was measured in the temperature range between 90 μK and 300 K using different experimental arrangements. At temperatures between 1.6 and 300 K the static magnetic susceptibility was measured in a commercial SQUID magnetometer at

Table 1. Refined values of the lattice parameters of ε-WO_3. In the 'Run' column, L indicates a long measurement and S indicates a shorter measurement; $\uparrow$ indicates a heating run, and $\downarrow$ indicates a cooling run.

T (K)	Run	a (Å)	b (Å)	c (Å)	β (deg)
5	↑L	5.277 10(1)	5.155 41(1)	7.662 97(1)	91.7592(2)
20	↑S	5.277 09(3)	5.155 44(3)	7.662 97(3)	91.7590(6)
30	↑S	5.277 14(3)	5.155 40(3)	7.663 04(3)	91.7587(6)
40	↑L	5.277 11(1)	5.155 48(1)	7.663 10(1)	91.7586(2)
50	↑S	5.277 07(3)	5.155 53(3)	7.663 24(3)	91.7573(6)
60	↑S	5.277 12(3)	5.155 59(3)	7.663 40(3)	91.7567(6)
70	↑L	5.277 13(1)	5.155 72(1)	7.663 69(1)	91.7555(2)
80	↑S	5.277 11(3)	5.155 92(3)	7.664 00(3)	91.7526(6)
90	↑S	5.277 06(3)	5.156 08(3)	7.664 40(3)	91.7505(6)
100	↑L	5.277 13(1)	5.156 30(1)	7.664 85(1)	91.7491(2)
110	↑S	5.277 11(3)	5.156 55(3)	7.665 40(3)	91.7445(6)
120	↑S	5.277 10(3)	5.156 92(3)	7.666 00(3)	91.7420(6)
130	↑L	5.277 17(1)	5.157 17(1)	7.666 59(1)	91.7373(2)
140	↑S	5.277 17(3)	5.157 57(3)	7.667 28(3)	91.7326(6)
140	↓L	5.277 26(1)	5.157 51(1)	7.667 27(1)	91.7332(2)
150	↑S	5.277 29(3)	5.157 97(3)	7.667 93(3)	91.7282(6)
150	↓L	5.277 30(1)	5.157 92(1)	7.667 97(1)	91.7292(2)
160	↑L	5.277 31(1)	5.158 39(1)	7.668 73(1)	91.7234(2)
170	↑S	5.277 36(3)	5.158 89(3)	7.669 51(3)	91.7165(6)
170	↓L	5.277 38(1)	5.158 73(1)	7.669 48(1)	91.7185(2)
180	↑L	5.277 42(1)	5.159 31(1)	7.670 36(1)	91.7127(2)
190	↑L	5.277 48(1)	5.159 77(1)	7.671 20(1)	91.7067(2)
200	↑L	5.277 57(1)	5.160 27(1)	7.672 04(1)	91.7009(2)
210	↑L	5.277 60(1)	5.160 78(1)	7.672 96(1)	91.6952(2)
220	↑S	5.277 69(3)	5.161 29(3)	7.673 97(3)	91.6884(6)
220	↓L	5.277 66(1)	5.161 24(1)	7.674 02(1)	91.6890(2)
230	↑L	5.277 70(1)	5.161 85(1)	7.674 95(1)	91.6824(2)
240	↑S	5.277 82(3)	5.162 38(3)	7.676 05(4)	91.6751(5)
240	↓L	5.277 48(2)	5.162 02(2)	7.675 68(3)	91.6758(4)
250	↑L	5.277 54(2)	5.162 57(2)	7.676 843)	91.6701(5)

a field strength of 1 T. In addition, the ac susceptibility ($\nu = 16$ Hz) was measured at $B \leqslant 0.1$ mT at temperatures between 1.6 and 40 K. At lower temperatures, 90 μK $\leqslant T \leqslant$ 6 K, the ac susceptibility was determined at $B \leqslant 0.01$ mT with a susceptometer mounted in a nuclear demagnetization refrigerator at the University of Bayreuth [32]. The samples used were taken from the same batch of material as was used in the neutron diffraction measurements.

The sample measured with the SQUID consisted of 130 mg of WO_3 crystals which were embedded in a gelatine capsule. The measured signal was corrected with respect to the temperature-independent signal of the gelatine capsule. Measurements in the millikelvin and microkelvin temperature ranges were conducted on cylinders of WO_3 mixed with the silver paste 'Stycast', an epoxy resin containing silver.

3. Rietveld refinement of the crystal structure of ε-WO_3

The Rietveld refinement of the crystal structure was performed using the ISIS in-house crystallographic software, which was developed specially for high-resolution time-of-flight

Table 2. Refined values of the fractional atomic coordinates and temperature factors for the W atoms of ε-WO_3. The x- and z-coordinates for W3 are determined by symmetry and were set at 1/2 and 3/4 respectively. ↑ indicates a heating run, and ↓ indicates a cooling run.

T (K)	W1 x	W1 y	W1 z	W3 y	B (Å^2)
5↑	−0.0099(5)	−0.020(1)	0.6743(2)	0.479(1)	−0.06(3)
20↑	−0.0128(9)	−0.012(1)	0.6744(4)	0.471(1)	−0.09(3)
30↑	−0.0146(9)	−0.010(2)	0.6749(4)	0.469(2)	−0.02(5)
40↑	−0.0129(5)	−0.013(1)	0.6744(2)	0.471(1)	−0.09(3)
50↑	−0.0117(9)	−0.018(2)	0.6741(4)	0.476(2)	−0.10(5)
60↑	−0.0135(9)	−0.010(2)	0.6750(4)	0.468(2)	−0.13(5)
70↑	−0.0118(5)	−0.013(1)	0.6748(2)	0.471(1)	−0.02(3)
80↑	−0.0114(9)	−0.014(2)	0.6754(4)	0.471(2)	−0.10(5)
90↑	−0.0135(9)	−0.014(2)	0.6745(4)	0.471(2)	−0.06(5)
100↑	−0.0121(5)	−0.011(1)	0.6749(2)	0.468(1)	−0.06(3)
110↑	−0.0133(9)	−0.009(2)	0.6742(4)	0.468(2)	−0.11(5)
120↑	−0.0110(9)	−0.017(2)	0.6742(4)	0.474(2)	−0.04(5)
130↑	−0.0129(5)	−0.010(1)	0.6745(2)	0.468(1)	−0.05(3)
140↑	−0.0112(9)	−0.013(2)	0.6743(4)	0.471(2)	0.00(5)
140↓	−0.0125(5)	−0.011(1)	0.6743(2)	0.470(1)	−0.01(3)
150↑	−0.0128(9)	−0.020(2)	0.6750(4)	0.477(2)	0.02(5)
150↓	−0.0129(5)	−0.015(1)	0.6746(2)	0.473(1)	0.04(3)
160↑	−0.0131(5)	−0.014(1)	0.6744(2)	0.473(1)	0.02(3)
170↑	−0.0121(9)	−0.010(2)	0.6745(4)	0.467(2)	−0.09(5)
170↓	−0.0130(5)	−0.014(1)	0.6747(2)	0.473(1)	0.06(3)
180↑	−0.0124(5)	−0.012(1)	0.6747(2)	0.471(1)	0.01(3)
190↑	−0.0120(5)	−0.016(1)	0.6748(2)	0.474(1)	0.06(3)
200↑	−0.0120(5)	−0.013(1)	0.6752(2)	0.471(1)	0.06(3)
210↑	−0.0119(5)	−0.013(1)	0.6748(2)	0.472(1)	0.04(3)
220↑	−0.0121(9)	−0.019(2)	0.6752(4)	0.478(2)	0.01(5)
220↓	−0.0111(5)	−0.012(1)	0.6745(2)	0.470(1)	0.07(3)
230↑	−0.0110(5)	−0.010(1)	0.6752(2)	0.470(1)	0.03(3)
240↑	−0.011(1)	−0.015(2)	0.6749(5)	0.474(2)	0.23(6)
240↓	−0.017(1)	−0.022(1)	0.676 77(6)	0.474(1)	0.25(5)
250↑	−0.014(1)	−0.022(2)	0.6754(7)	0.475(2)	0.28(6)

data with the characteristic lineshapes obtained with spallation neutron sources. The software allows for the refinements of more than one component structure from a single diffraction pattern. The background of the diffraction pattern was modelled using Chebyshev polynomials.

Since only the positions of the W atoms in the ε-phase have previously been determined [29], the strategy for the first refinement, which was performed using the data for ε-WO_3 at 5 K, needed to proceed fairly carefully in order to ensure convergence of the oxygen positions. We gave trial oxygen positions that corresponded to their values in the ideal cubic aristotype structures. During the first stage of the structure refinement we allowed the fractional coordinates of three of the six independent oxygen atoms to be varied to give the minimum value of the least-squares residual. In the next stage the fractional coordinates of all of the oxygen atoms were allowed to vary, and these quickly (i.e. within five least-squares cycles) locked into stable values. The value of χ^2 fell from its initial value of 72, obtained when only the cell parameters, scale factor and background parameters had been optimized, to a value of 3.2 before the W positions or the temperature factors had been varied. After the fractional coordinates of the oxygen atoms had been adjusted, the refinements were

Table 3. Refined values of the fractional atomic coordinates and temperature factors for the O atoms of ε-WO_3. ↑ indicates a heating run, and ↓ indicates a cooling run.

T (K)	O1 x	O1 y	O1 z	O2 x	O2 y	O2 z
5↑	0.492(2)	0.578(1)	−0.023(1)	0.213(2)	0.289(1)	0.183(1)
20↑	0.498(3)	0.581(2)	−0.031(2)	0.211(3)	0.298(2)	0.175(2)
30↑	0.494(3)	0.582(2)	−0.026(2)	0.205(3)	0.293(2)	0.179(2)
40↑	0.498(2)	0.584(1)	−0.029(1)	0.207(2)	0.294(1)	0.179(1)
50↑	0.498(3)	0.584(2)	−0.033(2)	0.209(3)	0.297(2)	0.172(2)
60↑	0.497(3)	0.579(2)	−0.028(2)	0.209(3)	0.293(2)	0.180(2)
70↑	0.496(2)	0.584(1)	−0.029(1)	0.207(2)	0.293(1)	0.177(1)
80↑	0.503(3)	0.582(2)	−0.022(2)	0.212(3)	0.288(2)	0.180(2)
90↑	0.501(3)	0.582(2)	−0.022(2)	0.210(3)	0.295(2)	0.180(2)
100↑	0.499(2)	0.584(1)	−0.026(1)	0.210(2)	0.293(1)	0.179(1)
110↑	0.498(3)	0.583(2)	−0.031(2)	0.210(3)	0.295(2)	0.175(2)
120↑	0.492(3)	0.584(2)	−0.032(2)	0.208(3)	0.295(2)	0.174(2)
130↑	0.496(2)	0.583(1)	−0.031(1)	0.209(2)	0.294(1)	0.178(1)
140↑	0.496(3)	0.582(2)	−0.031(2)	0.207(3)	0.297(2)	0.175(2)
140↓	0.496(2)	0.583(1)	−0.028(1)	0.208(2)	0.294(1)	0.179(1)
150↑	0.487(3)	0.584(2)	−0.034(2)	0.202(3)	0.296(2)	0.171(2)
150↓	0.495(2)	0.583(1)	−0.028(1)	0.206(2)	0.295(1)	0.176(1)
160↑	0.493(2)	0.583(1)	−0.031(1)	0.206(2)	0.294(1)	0.174(1)
170↑	0.499(3)	0.583(2)	−0.027(2)	0.211(3)	0.293(2)	0.178(2)
170↓	0.495(2)	0.583(1)	−0.028(1)	0.209(2)	0.295(1)	0.177(1)
180↑	0.495(2)	0.584(1)	−0.029(1)	0.209(2)	0.295(1)	0.179(1)
190↑	0.494(2)	0.583(1)	−0.029(1)	0.208(2)	0.296(1)	0.178(1)
200↑	0.495(2)	0.583(1)	−0.026(1)	0.211(2)	0.294(1)	0.179(1)
210↑	0.493(2)	0.584(1)	−0.028(1)	0.210(2)	0.295(1)	0.178(1)
220↑	0.489(3)	0.583(2)	−0.037(2)	0.199(3)	0.297(2)	0.167(2)
220↓	0.492(2)	0.582(1)	−0.032(1)	0.201(2)	0.298(1)	0.174(1)
230↑	0.497(2)	0.582(1)	−0.028(1)	0.210(2)	0.294(1)	0.179(1)
240↑	0.493(3)	0.583(1)	−0.032(2)	0.202(3)	0.296(1)	0.176(1)
240↓	0.490(2)	0.586(1)	−0.035(2)	0.192(1)	0.298(1)	0.168(2)
250↑	0.491(2)	0.586(1)	−0.036(1)	0.195(2)	0.298(1)	0.169(1)

performed allowing the fractional positions of the W atoms to vary (fixing the x- and z-positions of W1 at the values given by Salje [29] since the origin is not defined in the space group Pc), together with a single isotropic temperature factor for all of the W atoms and a second isotropic temperature factor for the O atoms, and lineshape parameters associated with the peak broadening due to the sample characteristics. The lineshape programmed into the in-house crystallographic software takes explicit account of a number of different contributions to the peak broadening. This led to a value for χ^2 of 3.0. In the final stage of the refinement we also refined a parameter associated with attenuation of the neutron beam by the sample, and a parameter associated with preferred orientation. Some preferred orientation might be expected because, as we have stated above, we were careful not to grind the sample too finely. Although the effects of preferred orientation were not large, allowing for this in the refinement gave a modest improvement on the final agreement between the observed and calculated diffraction patterns, leading to a final value for χ^2 of 1.6. For each of the long runs the Rietveld refinement converged to values for χ^2 of around 1.6 and R-factors of around 5%, and for each of the shorter runs the converged refinements had final values of χ^2 of around 1.1 and R-factors of around 9%. Over the range of data there are in excess of 650 independent Bragg reflections. It is interesting to note that with

Table 3. (Continued)

T (K)	O3 x	O3 y	O3 z	O4 x	O4 y	O4 z
5↑	0.283(2)	0.786(1)	0.259(1)	0.705(2)	0.207(1)	0.182(1)
20↑	0.282(3)	0.779(2)	0.252(2)	0.708(3)	0.207(2)	0.174(2)
30↑	0.276(3)	0.784(2)	0.257(2)	0.700(3)	0.203(2)	0.183(2)
40↑	0.278(2)	0.782(1)	0.256(1)	0.705(2)	0.202(1)	0.177(1)
50↑	0.280(3)	0.778(2)	0.249(2)	0.705(3)	0.203(2)	0.175(2)
60↑	0.279(3)	0.783(2)	0.257(2)	0.708(3)	0.206(2)	0.180(2)
70↑	0.277(2)	0.783(1)	0.254(1)	0.699(2)	0.203(1)	0.178(1)
80↑	0.283(3)	0.787(2)	0.257(2)	0.703(3)	0.206(2)	0.185(2)
90↑	0.280(3)	0.781(2)	0.256(2)	0.670(3)	0.204(2)	0.183(2)
100↑	0.280(2)	0.783(1)	0.255(1)	0.697(2)	0.206(1)	0.180(1)
110↑	0.280(3)	0.781(2)	0.253(2)	0.699(3)	0.206(2)	0.179(2)
120↑	0.277(3)	0.781(2)	0.251(2)	0.697(3)	0.199(2)	0.176(2)
130↑	0.280(2)	0.782(1)	0.254(1)	0.697(2)	0.205(1)	0.177(1)
140↑	0.279(3)	0.778(2)	0.251(2)	0.696(3)	0.205(2)	0.179(2)
140↓	0.278(2)	0.782(1)	0.255(1)	0.701(2)	0.205(1)	0.178(1)
150↑	0.273(3)	0.779(2)	0.247(2)	0.690(3)	0.201(2)	0.176(2)
150↓	0.277(2)	0.780(1)	0.252(1)	0.694(2)	0.202(1)	0.178(1)
160↑	0.276(2)	0.780(1)	0.250(1)	0.692(2)	0.202(1)	0.175(1)
170↑	0.281(3)	0.783(2)	0.254(2)	0.699(3)	0.208(2)	0.179(2)
170↓	0.279(2)	0.780(1)	0.253(1)	0.697(2)	0.202(1)	0.179(1)
180↑	0.279(2)	0.780(1)	0.254(1)	0.695(2)	0.204(1)	0.176(1)
190↑	0.278(2)	0.779(1)	0.253(1)	0.693(2)	0.202(1)	0.176(1)
200↑	0.280(2)	0.780(1)	0.254(1)	0.697(2)	0.203(1)	0.181(1)
210↑	0.279(2)	0.779(1)	0.253(1)	0.695(2)	0.203(1)	0.178(1)
220↑	0.270(3)	0.778(2)	0.243(2)	0.690(3)	0.203(2)	0.170(2)
220↓	0.272(2)	0.776(1)	0.249(1)	0.691(2)	0.205(1)	0.170(1)
230↑	0.278(2)	0.779(1)	0.254(1)	0.696(2)	0.206(1)	0.179(1)
240↑	0.271(3)	0.777(1)	0.251(2)	0.694(3)	0.201(1)	0.170(2)
240↓	0.260(2)	0.776(1)	0.242(2)	0.672(2)	0.206(1)	0.169(2)
250↑	0.265(2)	0.773(1)	0.243(1)	0.672(2)	0.208(1)	0.166(2)

the oxygen atoms in their starting positions, the two strong peaks in the diffraction patterns with largest d-spacings (see figure 1), corresponding to the 013 reflection at 110.6 ms, and a doublet of the $\bar{1}21$ and 211 reflections at 107.53 ms (the two components are actually almost resolved in the diffraction patterns), are calculated to have almost zero intensity. Despite such large discrepancies between the initial calculated diffraction pattern and the observed diffraction pattern, the Rietveld refinement quickly converged to the final stable structure with the oxygen atoms displaced from their initial positions. We checked that the refinement was converging to a true minimum by using a variety of different starting points with random displacements of the oxygen atoms from the initial ideal positions, obtaining the same result in each case.

For the data at high temperatures, which contained diffraction patterns from both the monoclinic ε- and triclinic δ-phases, we performed a multi-phase refinement, in which the structural parameters of both phases can, at least in principle, be adjusted simultaneously, together with a parameter that gives the relative proportions of the two components. The results of multi-phase refinements cannot be as accurate as those from single-phase refinements. In our case, it was not possible to obtain convergence of the refinements of both phases when all of the structural parameters were adjusted together. Because the δ-phase was the minority component, we adjusted all of the structural parameters of the ε-

Table 3. (Continued)

T (K)	O5 x	O5 y	O5 z	O6 x	O6 y	O6 z	B (Å^2)
5↑	0.796(2)	0.711(1)	0.261(1)	−0.012(2)	0.073(1)	0.463(1)	0.18(2)
20↑	0.797(3)	0.712(2)	0.252(2)	−0.006(3)	0.071(2)	0.454(2)	0.22(4)
30↑	0.790(3)	0.715(2)	0.260(2)	−0.012(3)	0.069(2)	0.458(2)	0.29(4)
40↑	0.796(2)	0.716(1)	0.255(1)	−0.009(2)	0.068(1)	0.456(1)	0.21(2)
50↑	0.796(3)	0.714(2)	0.253(2)	−0.009(3)	0.069(2)	0.452(2)	0.14(4)
60↑	0.799(3)	0.714(2)	0.258(2)	−0.008(3)	0.073(2)	0.457(2)	0.19(4)
70↑	0.791(2)	0.716(1)	0.255(1)	−0.009(2)	0.068(1)	0.456(1)	0.26(2)
80↑	0.794(3)	0.713(2)	0.262(2)	−0.003(3)	0.069(2)	0.462(2)	0.28(4)
90↑	0.790(3)	0.715(2)	0.260(2)	−0.004(3)	0.070(2)	0.462(2)	0.25(4)
100↑	0.788(2)	0.714(1)	0.257(1)	−0.008(2)	0.068(1)	0.458(1)	0.26(2)
110↑	0.789(3)	0.714(2)	0.256(2)	−0.006(3)	0.068(2)	0.455(2)	0.26(4)
120↑	0.788(3)	0.720(2)	0.252(2)	−0.014(3)	0.067(2)	0.452(2)	0.22(4)
130↑	0.787(2)	0.714(1)	0.254(1)	−0.009(2)	0.068(1)	0.455(1)	0.33(2)
140↑	0.785(3)	0.715(2)	0.256(2)	−0.008(3)	0.068(2)	0.454(2)	0.36(4)
140↓	0.792(2)	0.715(1)	0.254(1)	−0.009(2)	0.067(1)	0.457(1)	0.37(2)
150↑	0.778(3)	0.718(2)	0.253(2)	−0.017(3)	0.066(2)	0.451(2)	0.33(4)
150↓	0.784(2)	0.716(1)	0.254(1)	−0.010(2)	0.067(1)	0.457(1)	0.37(2)
160↑	0.783(2)	0.717(1)	0.251(1)	−0.012(2)	0.067(1)	0.454(1)	0.32(2)
170↑	0.790(3)	0.713(2)	0.255(2)	−0.006(3)	0.067(2)	0.458(2)	0.37(4)
170↓	0.788(2)	0.716(1)	0.255(1)	−0.010(2)	0.066(1)	0.457(1)	0.37(2)
180↑	0.785(2)	0.716(1)	0.252(1)	−0.011(2)	0.066(1)	0.456(1)	0.36(2)
190↑	0.782(2)	0.717(1)	0.252(1)	−0.011(2)	0.067(1)	0.456(1)	0.37(2)
200↑	0.788(2)	0.716(1)	0.257(1)	−0.011(2)	0.066(1)	0.459(1)	0.42(2)
210↑	0.786(2)	0.716(1)	0.254(1)	−0.012(2)	0.066(1)	0.456(1)	0.40(2)
220↑	0.778(3)	0.717(2)	0.246(2)	−0.016(3)	0.067(2)	0.449(2)	0.41(4)
220↓	0.779(2)	0.714(1)	0.246(1)	−0.013(2)	0.067(1)	0.454(1)	0.45(2)
230↑	0.786(2)	0.714(1)	0.255(1)	−0.009(2)	0.066(1)	0.457(1)	0.45(2)
240↑	0.783(3)	0.718(1)	0.246(2)	−0.011(3)	0.065(1)	0.454(2)	0.54(5)
240↓	0.761(2)	0.713(1)	0.244(2)	−0.015(2)	0.063(1)	0.447(2)	0.53(2)
250↑	0.760(2)	0.709(1)	0.241(2)	−0.014(2)	0.063(1)	0.447(2)	0.53(3)

Table 4. Refined values of the lattice parameters and phase fractions of δ-WO_3.

	240 K	250 K
a (Å)	7.3090(3)	7.3091(3)
b (Å)	7.5165(3)	7.5176(3)
c (Å)	7.6811(3)	7.6823(3)
α (deg)	88.811(1)	88.820(1)
β (deg)	90.949(1)	90.944(1)
χ (deg)	90.985(2)	90.976(2)
Phase fraction	0.150(1)	0.200(1)

phase together with the cell parameters and a few other structural parameters of the δ-phase (the fixed values were taken from the previous structure determination [31]), with our sole objective being to determine the structure of the ε-phase, using the multi-phase refinement to extract the relevant part of the total diffraction pattern.

The final calculated diffraction pattern for the structure at 5 K is compared with the corresponding experimental data in figure 1. The refined values of the lattice parameters of the ε-phase for each temperature are given in table 1, and the refined fractional atomic

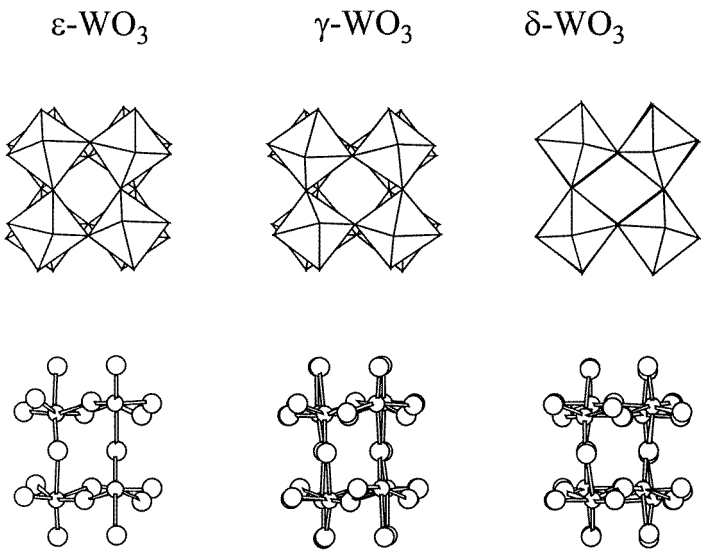

Figure 2. Principle features of the crystal structures of the three low-temperature phases of WO_3 (the monoclinic ε-phase, space group Pc, the triclinic δ-phase, space group $P\bar{1}$, and the monoclinic δ-phase, space group $P2_1/n$) showing the tilting of the WO_6 octahedra (top) and the W–O bonds (bottom). The views for the polyhedral representations of the ε-, δ- and γ-phases are down [001], [001] and [010] respectively, and each shows two layers. Note that the rotations in the two layers are in opposite directions in the ε- and δ-phases, but in the same direction in the γ-phase. The views for the atom and bond representations of the ε-, δ- and γ-phases are down [100], [110] and [101] respectively, with the [001], [001] and [010] axes upwards. The structure of the ε-phase is taken from this paper, and those of the other phases from references [31] and [34].

coordinates and isotropic temperature factors are given in table 2 (W atoms) and table 3 (O atoms). At the lower temperatures the temperature factor for the W atoms is negative, which is a common indication that the effects of absorption of the neutron beam have not been adequately handled in our data reduction and refinement. The refined values of the lattice parameters of the δ-phase at 240 K and 250 K are given in table 4.

4. Discussion of the crystal structure of ε-WO_3

4.1. Details of the crystal structure of ε-WO_3 compared to the other low-temperature phases

The crystal structure of ε-WO_3 at 5 K is shown in figure 2, which highlights both the tilting of the WO_6 octahedra from their orientations in the ideal cubic aristotype structure, and the distortions of the WO_6 octahedra caused by the displacements of the W atoms away from the centres of the octahedra. From figure 2 it can be seen that the orientations of the WO_6 octahedra can be related to their orientations in the ideal cubic aristotype structure by two rotations. The first is the rotation about the monoclinic c-axis (which is parallel to the [0, 0, 1] axis in the cubic phase, but twice as long), and the second is a rotation about the monoclinic a-axis. The latter axis corresponds to the [1, 1, 0] direction in the cubic phase, which suggests that the tilt about this axis can be resolved as the sum of tilts of equal size about the [1, 0, 0] and [0, 1, 0] axes of the cubic phase. Thus, in Glazer's notation [33], the rotational distortion of the cubic phase can be written as $a^-a^-c^-$. Glazer has shown that

this leads to a centrosymmetric monoclinic structure of space group $I2/c$ [33]. In ε-WO_3 the symmetry is lowered to the space group Pc by the displacements of the W atoms from the centres of the WO_6 octahedra: in figure 2 the octahedra at the origin and at the centre of the unit cell would be equivalent in a $I2/c$ structure. We have calculated tilt angles at 5 K of 16.4° about the cubic [0, 0, 1] axis, and 5.1° about the cubic [1, 0, 0] and [0, 0, 1] axes.

The pattern of octahedral tilts can be compared with the tilts in the other two low-symmetry phases, which are also shown in figure 2. The most striking contrast is with the monoclinic γ-phase, space group $P2_1/n$, where it is clear that along [0, 0, 1] the rotations are the same in consecutive layers, corresponding to the tilt system $a^-a^-c^+$. On the other hand, the pattern of tilts in the triclinic δ-phase, space group $P\bar{1}$ [31], is similar to that of the ε-phase, as is clearly seen in figure 2, but the actual rotations about the three axes are not approximately equal, so the tilt pattern is better described as $a^-b^-c^-$. However, one should admit that with small distortions of the octahedra and limited precision one can never exactly distinguish between $a^-a^-c^-$ and $a^-b^-c^-$ when rotations are similar.

We now consider the shapes of the WO_6 octahedra in the three low-symmetry phases of WO_3. Although there is a spread of W–O bond lengths in WO_3, a large part of this arises from the displacements of the W cations from the centres of the WO_6 octahedra. To quantify the actual distortions of the octahedra, we define the centre of mass of the oxygen atoms by the point $\boldsymbol{X}$, and have calculated the $\boldsymbol{X}$–O distances and O–$\boldsymbol{X}$–O angles. The results for the three phases are given in table 5.

Table 5. Centre-of-mass distances and angles for the three low-temperature phases of WO_3. Definitions are given in the text.

	$P2_1/n$		Pc		$P\bar{1}$			
Mean $\boldsymbol{X}$–O bond length (Å)	1.91	1.91	1.90	1.92	1.91	1.92	1.92	1.90
Spread of $\boldsymbol{X}$–O bond lengths (Å)	0.04	0.04	0.06	0.03	0.06	0.06	0.04	0.03
Spread of O–$\boldsymbol{X}$–O angles (deg)	1.7	1.4	1.9	1.0	1.6	1.8	2.0	2.3

The spread of the $\boldsymbol{X}$–O distances only amounts to 2–3 %, and is not significantly larger than the level of precision given by the crystal structure refinements. The spread of the O–$\boldsymbol{X}$–O angles is within 2°. These quantities indicate that in these three phases there are only minimal distortions of the O_6 octahedra.

The displacements of the W atoms from the centres of the octahedra are highlighted in figure 2. The displacements are in the directions of some of the faces of the octahedra. In figure 2 we show the pattern of long and short W–O bonds along the monoclinic [0, 0, 1] axis: this is the most extreme pattern. The space group of the ε-phase, Pc, does not have a centre of symmetry, and therefore the unit cell will have a non-vanishing electric dipole moment. The dipole moments associated with each W site arising from the surrounding O atoms have been calculated on the basis of a coordinate system where x is parallel to [1, 0, 0], y is parallel to [0, 1, 0], and z is parallel to $\boldsymbol{c}^*$, and assigning a single electronic unit of charge to each oxygen in a WO_6 octahedron (noting that each oxygen contributes to two octahedra, so the formal charge of two electron units has been halved). The results have been averaged over all of the structure refinements from the longer diffraction runs in order to minimize errors, and for the two independent W sites the results are given in table 6 (in units of e Å^2).

The smallest components, along x, more or less cancel over the unit cell. The largest components, along z, also cancel, leaving a small residual moment. On the other hand, the

Table 6. Calculated electric dipole moments on the WO_6 octahedra in ε-WO_3 arising from the displacements of the W ions (in units of e Å^2).

	x	y	z
W(1)O_6	−0.08(5)	−0.43(6)	−1.74(5)
W(3)O_6	0.15(5)	−0.92(6)	1.48(6)
Sum	0.07(7)	−1.35(9)	−0.26(8)

moments along y of the two octahedra are of the same sign, but the symmetry of the space group, with the equivalent positions x, y, z, and $x, -y, 1/2+z$, means that the net moment along y must be exactly zero. Thus the final moment on the unit cell is primarily along z, and summed over the four W sites is 0.52 ± 0.16 e Å^2.

The calculations of the dipole moments highlight the fact that the largest displacements of the W cations are along the z-direction. These are highlighted in figure 2, from which it can be seen that there is an alternating pattern of long and short W–O bonds along z. In this figure we compare the same pattern for the other two phases, and it is clear that the pattern of long and short bonds is more exaggerated in the ε-phase.

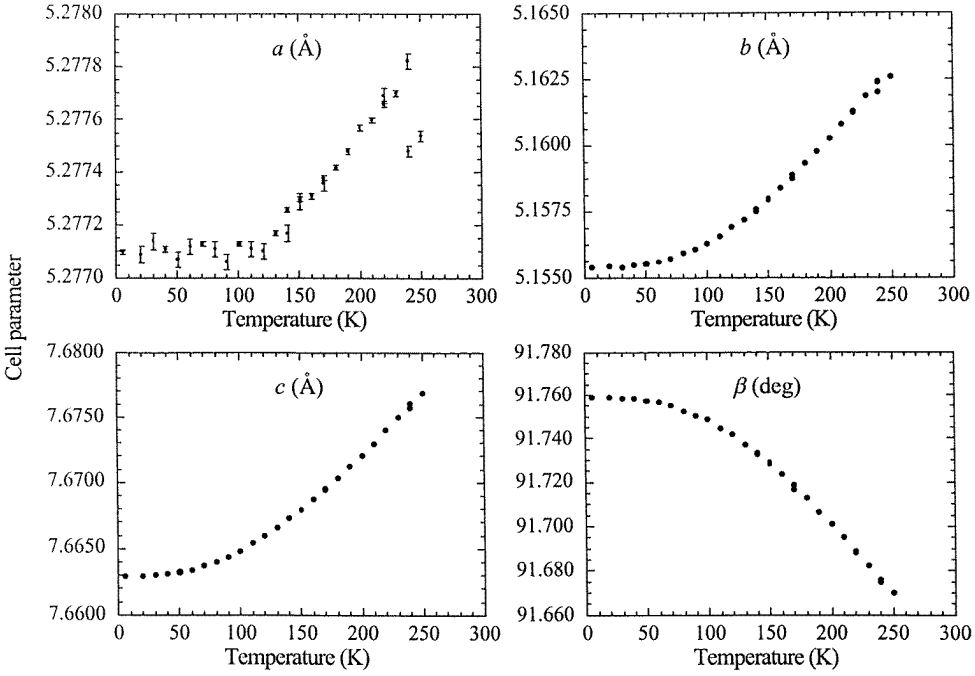

Figure 3. Temperature dependences of the lattice parameters of ε-WO_3.

4.2. Temperature dependence of the crystal structure of ε-WO_3

The temperature dependences of the lattice parameters are shown in figure 3. There are two important points to note from these figures. The first is that there is only a weak temperature

dependence in each case. In particular, there is no sign of rapid changes on heating towards the ε–δ phase transition. Second, there are no signs of any other phase transitions occurring below 220 K. The structural data point to a single phase occurring for all temperatures below 220 K without any significant variations with temperature. The atomic coordinates similarly show only a weak dependence on temperature. The dipole moments do not show any variation with temperature within the errors imposed by the precision of the structure refinements.

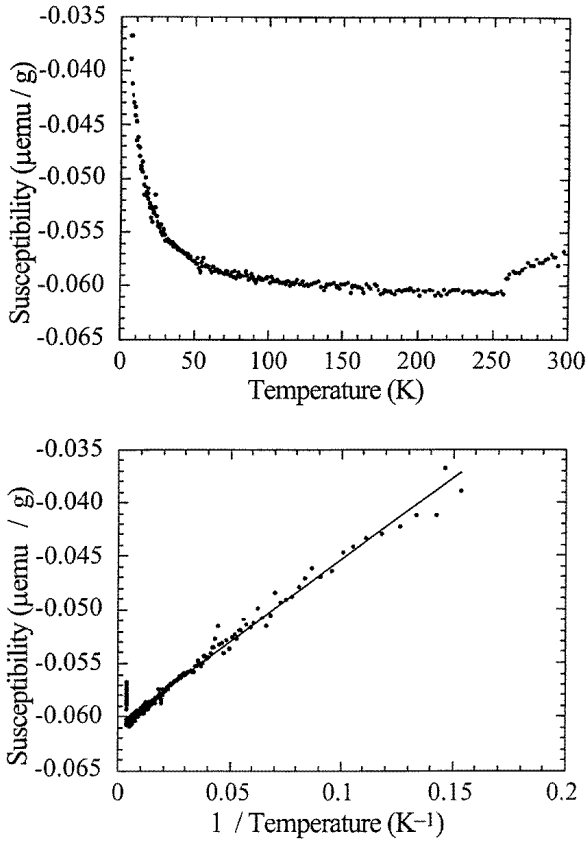

Figure 4. Temperature dependences of the static susceptibility of WO_3 plotted as functions of temperature (top) and inverse temperature (bottom). The susceptibility has a constant diamagnetic contribution with a Curie paramagnetic component. The measurements were performed in a field of 1 T.

5. The magnetic susceptibility of ε-WO_3

The static magnetic susceptibility of WO_3 is shown in figure 4. The data, which are dominated by the diamagnetic contribution, show two dominant features. The first is a step at the transition point between the δ-phase and the ε-phase. The susceptibility increases with increasing temperature in the δ-phase. The second feature is that in the ε-phase there

is a characteristic Curie paramagnetic contribution to the susceptibility, with

$$\chi = \chi_0 + \frac{C}{T}.$$

The value of the Curie constant C obtained by fitting to the experimental data is 0.155 ± 0.001 μemu K g^{-1}, and the fitted value of the diamagnetic susceptibility χ_0 is -0.0608 ± 0.0001 μemu g^{-1}. Magnetization measurements were performed at magnetic field strengths of 4 T in order to determine the size of the magnetic moments, and the results implied a size of 4 μ_B.

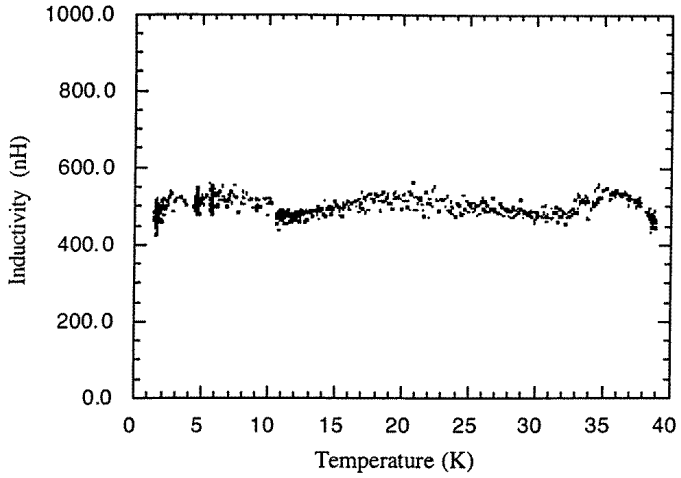

Figure 5. The AC magnetic susceptibility of WO_3 measured as a function of temperature for field strengths below 0.1 mT. The background signals have been subtracted.

The real part of the ac magnetic susceptibility measured for $B < 0.1$ mT and with the background signal subtracted is shown in figure 5. It is clear that the susceptibility is independent of temperature over the whole temperature range. In order to check whether superconductivity is suppressed by a critical magnetic field, the sample was scanned at $T = 90$ μK in a field between -0.30 mT and 0.64 mT. The accuracy of the field measurement was 0.01 mT. The inductivity of the sample was found to be completely independent of the magnetic field strengths throughout the range of the measurements, no magnetic anomalies were observed, and no indication for a superconducting phase transition was found.

6. Discussion of the magnetic susceptibility data

The decrease in the susceptibility during the δ–ε phase transition is similar to the behaviour occurring during the metal–insulator transitions in V_2O_5 and Ti_4O_7. It has been argued that the step in the susceptibility is directly correlated with the change of the effective mass of the Pauli susceptibility, although there is also a temperature dependence of the diamagnetic background susceptibility due to the structural changes driving the δ–ε phase transition. A clear separation of the two effects appears difficult, although an increase of the susceptibility in the metallic phase appears to be a general phenomenon in metal–insulator transitions, and therefore may not be entirely related to subtle structure changes.

The Curie behaviour in the ε-phase has to be seen in conjunction with the results of ESR experiments by Schirmer and Salje [24]. In these experiments it was found that only a very weak ESR signal exists at 20 K, which is strongly increased by illumination of the sample. This effect was attributed to the optical excitation of bipolarons into two single polarons. The total concentration of ESR-active carriers in the illuminated samples used by Schirmer and Salje [24] was 1.27×10^{19} cm^{-3}. The dark samples showed only very weak ESR signals, so the paramagnetic centres would exist with concentrations less than $\simeq 10^{18}$ cm^{-3}. The carrier concentrations in the samples in the measurements reported in this paper can be obtained from the measurements of the diamagnetic susceptibility. The magnetization measurements suggest that the carriers are paramagnetic triplet states, i.e. two W^{5+} with parallel spins of net moment 4 μ_B. The measurements give a carrier concentration of 0.33×10^{18} cm^{-3}. Both concentrations are lower than the typical total carrier concentration which is incorporated in the temperature-independent background. The thermal activation of singlet states into triplet states may well explain the weak increase of the susceptibility with increasing temperature in the δ-phase. No significant effect of thermal triplet excitation was found in the ε-phase.

Acknowledgments

The work involving the magnetic susceptibility measurements was supported by the Large Scale Facility Programme of the European Community under Contract number ERB-CHGE-CT 920002, and by the BMBF through Verbunprojekt PO 04.04 K. The neutron scattering measurements were supported by the EPSRC (UK).

References

[1] Mott N F 1990 *Adv. Phys.* **39** 55
[2] Alexandrov A S 1987 *JETP Lett. Suppl.* **46** 107
[3] Alexandrov A S 1982 *J. Low Temp. Phys.* **87** 721
[4] Alexandrov A S and Ranninger J 1992 *Solid State Commun.* **81** 403
[5] Mott N F 1992 *Physica* C **196** 369
[6] Alexandrov A S and Ranninger J 1989 *Physica* C **159** 367
[7] Ohbi H S and Salje E K H 1992 *J. Phys.: Condens. Matter* **4** 195
[8] Ohbi H S and Salje E K H 1990 *Physica* C **141** 547
[9] Alexandrov A S 1992 *Phys. Rev.* B **46** 14 932
[10] Ranninger J 1991 *Z. Phys.* B **84** 167
[11] Robaszkiewicz S, Micknas R and Ranninger J 1987 *Phys. Rev.* B **36** 180
[12] Emin D and Hillery M S 1989 *Phys. Rev.* B **39** 6575
[13] Obhi H S, Salje E K H and Miyatake T 1992 *J. Phys.: Condens. Matter* **4** 10 367
[14] Güttler B, Salje E, Freemann P, Blunt J, Harris M, Duffield T, Auge C D and Hughes H P 1991 *Supercond. Sci. Technol.* **4** S70
[15] Güttler B, Salje E, Freemann P, Blunt J, Harris M, Duffield T, Auge C D and Hughes H P 1990 *J. Phys.: Condens. Matter* **2** 8977
[16] Yagil Y and Salje E K H 1996 *Physica* C **256** 205
[17] Yagil Y, Baudenbacher F, Zhang M, Birch J R, Kinder H and Salje E K H 1995 *Phys. Rev.* B **52** 21
[18] Ranninger J 1993 *Phys. Rev.* B **48** 13 166
[19] Ranninger J 1991 *Phys. Scr.* T **39** 61
[20] Schirmer O F and Salje E 1980 *J. Phys. C: Solid State Phys.* **13** 1067
[21] Berak J M and Sienko M J 1970 *J. Solid State Chem.* **2** 109
[22] Gehlig R and Salje E 1983 *Phil. Mag.* B **47** 229
[23] Salje E and Hoppmann G 1981 *Phil. Mag.* B **43** 145
[24] Schirmer O F and Salje E 1980 *Solid State Commun.* **33** 333
[25] Salje E and Güttler B 1984 *Phil. Mag.* B **50** 607

[26] Yoshimura T 1985 *J. Appl. Phys.* **57** 911
[27] Salje E K H 1994 *Polarons and Bipolarons in High-T_c Superconductors and Related Materials* ed E K H Salje, A Alexandrov and Y Liang (Cambridge: Cambridge University Press) p 110
[28] Lefkowitz I, Dowell M B and Shields M A 1975 *J. Solid State Chem.* **15** 24
[29] Salje E 1976 *Ferroelectrics* **12** 215
[30] Salje E, Gehlig R and Viswanathan K 1978 *J. Solid State Chem.* **25** 239
[31] Diehl R, Brandt G and Salje E 1978 *Acta Crystallogr.* B **34** 1105
[32] Gloos K, Smeibidl P, Kennedy C, Singsaas A, Sekowski P, Mueller R M and Pobell F 1988 *J. Low Temp. Phys.* **73** 101
[33] Glazer A M 1972 *Acta Crystallogr.* B **28** 3384
[34] Tanisaki S 1960 *J. Phys. Soc. Japan* **15** 573